Science of the Total Environment 781 (2021) 146740

Contents lists available at ScienceDirect

Science of the Total Environment

journal homepage: www.elsevier.com/locate/scitotenv

Mineralogy of particulate inputs and P-speciation and mineralogy of recently accreted soils within Everglades stormwater treatment wetlands

Jonathan D. Judy [a,*], Willie Harris [a], Ganga M. Hettiarachchi [b], A. Caroline Buchanan [a], K. Ramesh Reddy [a]

[a] University of Florida, Soil and Water Sciences Department, 1692 McCarty Dr., Gainesville, FL 32611, USA
[b] Kansas State University, Department of Agronomy, 1712 Claflin Road, Throckmortonal Hall, Manhattan, KS 66506, USA

HIGHLIGHTS

- A strong autochthonous influence on wetland soil mineralogy was observed.
- P was associated with K and Ca in soil regardless of wetland vegetation.
- Apatitic minerals were detected in soil from both EAV and SAV cells.
- Apatitic minerals are less likely than more labile P to affect downstream conditions.

GRAPHICAL ABSTRACT

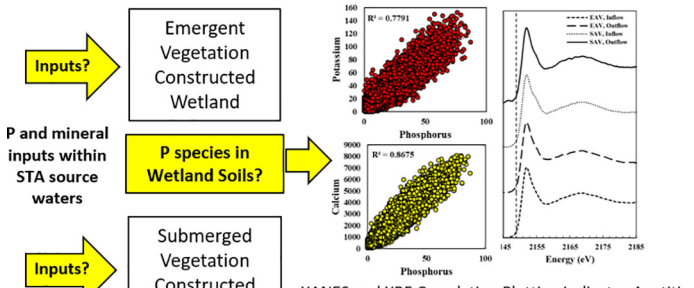

XANES and XRF Correlation Plotting Indicates Apatitic Minerals and Association between P and Ca/K in Both Types of Constructed Wetland Cells

ARTICLE INFO

Article history:
Received 10 December 2020
Received in revised form 15 March 2021
Accepted 21 March 2021
Available online 26 March 2021

Editor: Yucheng Feng

Keywords:
Biogeochemistry
Colloids
Phosphorus enrichment
XANES
XAS
Constructed wetlands
Non-point source pollution
Diffuse pollution

ABSTRACT

Phosphorus (P) biogeochemical processes in wetlands are influenced by the chemical composition of both recently accreted and native soils. The evaluation of biogeochemical processes influencing P transformations requires an understanding of the participating chemical components. Here, we use X-ray diffraction (XRD), scanning electron microscopy (SEM)/energy-dispersive X-ray fluorescence spectroscopy (EDS), X-ray absorption near-edge P spectroscopy (P-XANES), and microprobe X-ray fluorescence (μ-XRF) to examine the mineralogy and P speciation of solid phases entering and within selected Everglades Stormwater Treatment Areas (STAs). Suspended particulates in the source waters (upstream of the STAs) to the STAs were examined and compared with those of recently-accreted soil (RAS) from inflow, mid-flow, and outflow locations of two flowways (FWs) within STA-2: one dominated by emergent aquatic vegetation (EAV) and the other dominated by submerged aquatic vegetation (SAV). Source water particulates included carbonates and silicates, whereas mineralogies of STA RAS were less diverse, dominated by $CaCO_3$ and having a lower silicate content, suggesting a strong autochthonous influence on STA RAS composition. No P minerals were detected via XRD. Discrete Ca—P particles were evident, though uncommonly observed, in two of three STA RAS samples analyzed via SEM/EDS. P-XANES of STA RAS indicated the presence of apatitic minerals. The potential presence of apatitic minerals was supported by μ-XRF correlation analysis that revealed strong correlations of P with both Ca and K. Apatitic minerals are a relatively refractory form of P and their presence in the RAS of both EAV and SAV systems indicate that remobilization and release of this P from the STAs will have a smaller effect on the downstream oligotrophic conditions of the Florida Everglades than more labile forms of P.

* Corresponding author at: University of Florida, Soil and Water Sciences, 1692 McCarty Drive, 2181 McCarty Hall A, USA.
E-mail address: jonathan.judy@ufl.edu (J.D. Judy).

https://doi.org/10.1016/j.scitotenv.2021.146740
0048-9697/

1. Introduction

Anthropogenic phosphorus (P) loads from upstream watersheds are a long-term threat to the oligotrophic ecosystems of the Florida Everglades, a wetland of significant national interest. In the mid-1990s, the state of Florida developed a plan for reduction of P fluxes into the Everglades, which included the construction of six Stormwater Treatment Areas (STAs; Fig. 1; (Pant and Reddy, 2001)). These six treatment wetlands have an effective treatment area of over 275 km^2 and are subdivided into 35 treatment flowways (FWs). The STAs receive water with high concentrations of P (typically above 100 $\mu g\ L^{-1}$) from the Everglades Agricultural Area and Lake Okeechobee to the north and remove over 70% of this P prior to discharging the water into the Water Conservation Areas to the south (Mitsch et al., 2015).

While the STAs remove the majority of total P prior to discharge, outflow P still exceeds desired levels. The ability of STAs to reduce P fluxes is a complex process driven by numerous biological and chemical interactions that transform P into different forms (Chimney, 2019). While some forms of P are readily retained within the STAs, others with more complex structures or tightly bound to particulates are harder to break down and influence the ability of the STA to meet the required low outflow concentrations. Removal of additional P is challenging and is complicated by imperfect understanding of the phases and species contributing to the remaining P leaving the STAs.

Constructed wetlands are typically composed of emergent aquatic vegetation (EAV), submerged aquatic vegetation (SAV), or a mixture of the two. In the Everglades STAs, EAV is primarily cattail (*T. latifolia*) while SAV includes the macroalgae *Chara* (muskgrass), *Najas marina* (spiny water nympth), *and Najas guadalupensis* (southern water nymph) *and Ceratophyllum demersum* (hornwort) (Chen et al., 2015; Kadlec, 2006). The mechanisms of P removal are different between the two vegetation types, with the high organic P accumulating in soils of EAV-dominated areas and relatively high inorganic P accumulation in soils of SAV-dominated areas (Reddy et al., 2020). Roots of EAV access nutrients primarily from soil porewater, whereas the shoots and leaves of SAV generally obtain nutrients directly from the water column (Jerauld, 2010). Typically, constructed wetland flow paths are designed to have EAV at the front end, followed by SAV at the back end, which provides the final stage of nutrient removal.

A relatively high proportion of P entering treatment wetlands is often, as in the case with the STAs (Farve et al., 2004; Vymazal, 2007), in the form of suspended particulates r(Mendes et al., 2018). Inorganic and organic soil and sediment particles become suspended and entrained within water entering wetlands with potentially deleterious environmental consequences (Harris et al., 2007; Li et al., 2018; Lee et al., 2020). For example, suspended particles can absorb and scatter light, contributing to turbidity and a reduction in available light, which can lead to SAV limitation or die off (Bornette and Puijalon, 2011;

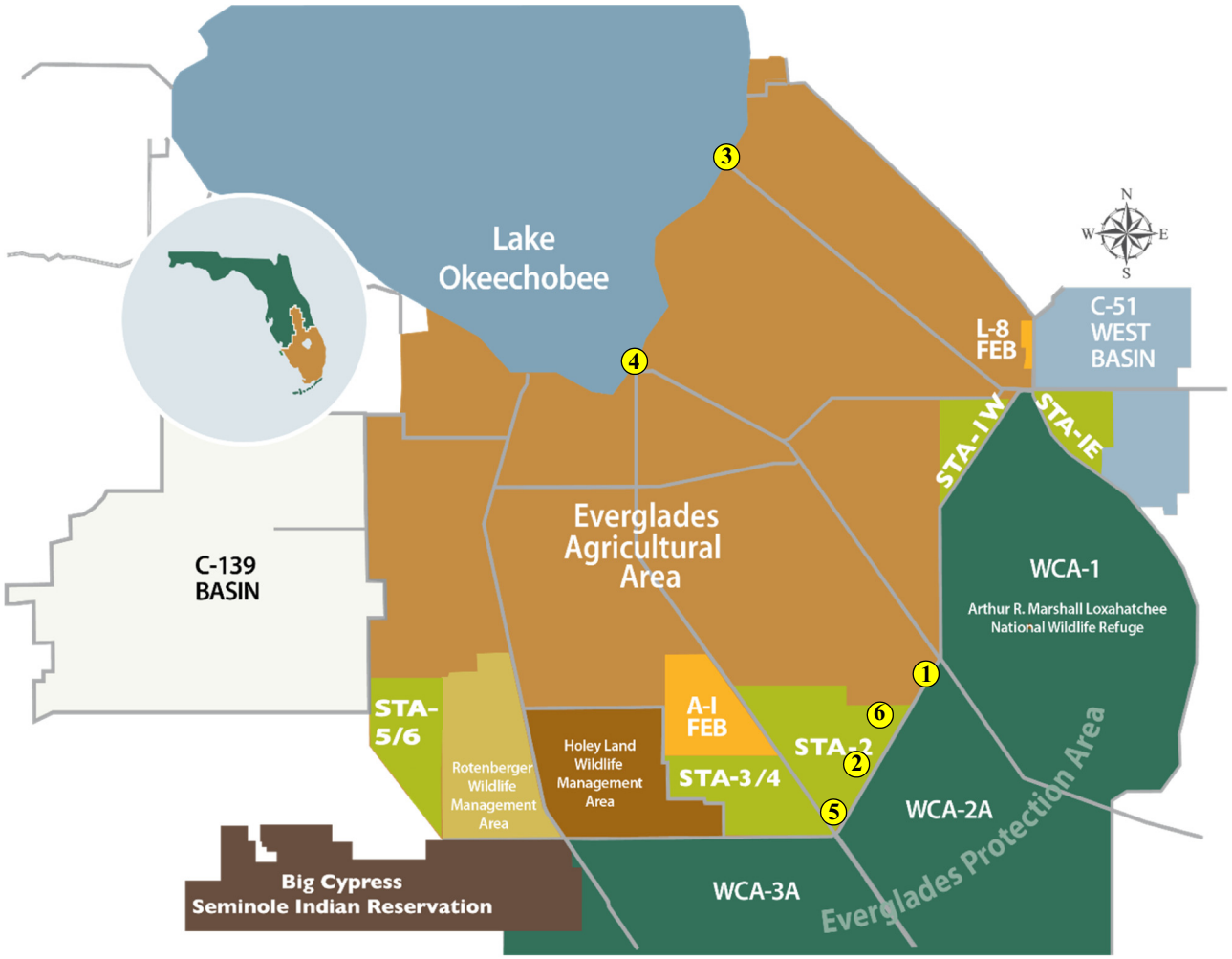

Fig. 1. Map of south Florida showing Lake Okeechobee, the Everglades Agricultural Area, the six Stormwater Treatment Areas (STAs), two associated Flow Equalization Basins (FEBs) and the Everglades Protection Area (EPA), which includes Water Conservation Areas (WCAs). Water flows from Lake Okeechobee and the Everglades Agricultural Area into the FEBs and STAs before being discharged into the EPA. Station 1- G328 – pumps EAA runoff into STA-2; Station 2- STA-2-FW 1 - midflow - sample was taken from the levee; Station 3 – S-352 Lake Okeechobee discharge structure; Station 4 – S-351 Lake Okeechobee discharge structure; Station 5 – G-330B-STA-2 FW 1 outflow; and Station 6 – G-329C -STA-2 FW 1 inflow.

Moore et al., 2012), the latter of which will result in release of nutrients back into the water column from the decomposition of plant tissue (Kroger et al., 2007). An increase in suspended particles in the water column has also been known to negatively affect oyster egg development and lead to increased mortality of estuarine fish larvae (Wilber and Clarke, 2001). Suspended particulates can also serve as vectors for the transport of dissolved nutrients (Judy et al., 2018; Makris et al., 2006) and contaminants (Xing et al., 2016). A portion of the suspended organic and inorganic particulates accumulates in the STA soils between inflow and outflow, resulting in a decreased total P concentration in the water column. Additional total P reduction is attributed to biogeochemical processes such as sorption, precipitation and/or plant uptake occurring within the STAs.

Understanding the biogeochemical processes influencing P dynamics requires an understanding of the participating chemical components. The objective of this study is to use X-ray diffraction (XRD) to characterize particulate components of source water samples, and XRD, and scanning electron microscopy (SEM)/energy-dispersive spectroscopy (EDS), X-ray absorbance near-edge spectroscopy (XANES) and X-ray fluorescence microprobe (μ-XRF) to characterize the mineral and organic components present in particulates within STA source waters and soils of STAs. XRD will enable characterization of the crystalline mineral phases present, whereas SEM/EDS and XRF will allow for spatially resolved analysis of elemental composition and P colocalization with other elements. P XANES will provide information as to the organic and inorganic P speciation within the sample. Furthermore, both XRF and XANES are more sensitive that SEM/EDS. These data will support understanding of P inputs and biogeochemical interactions among P species within different regions of the STAs. This work is an extension to recent work (Reddy et al., 2020) that reported P fractionation and ^{31} P NMR data collected from samples from the same RAS samples we examine here. Together, these analyses will provide novel and valuable information regarding the chemical composition of inputs and will infer the influence of these STAs on P dynamics, based on the changes in downstream soil composition.

2. Materials and methods

2.1. Source water sample collection, handling, and preparation

Water samples were collected mid-November 2015 at six locations just southeast of Lake Okeechobee (see Fig. 1 for sampling station locations and Fig. S1 for aerial maps of the locations of Stations 1, 2, 5 and 6) and transferred to the Soil Mineralogy Laboratory (Soil and Water Sciences Department, University of Florida). These six sampling locations included four locations where water leaving the Everglades Agricultural Area and flowing into the STAs was sampled (Fig. 1; Sites 1 (pumping station G-328), 2 (midflow from STA-2, FW 1, taken from the levee), 5 (pumping station G-330B near STA-2 outflow) and 6 (pumping station G-329C, near STA-2 inflow)), as well as two sites where Lake Okeechobee outflow was sampled (Fig. 1; Sites 3 (Lake Okeechobee discharge structure S-352) and 4 (Lake Okeechobee discharge structure S-351)). These sampling locations were selected to represent critical hydrologic junctures. Station 1 was at point of entry for Everglades Agricultural Area runoff into STA-2. Stations 3 and 4 were selected to represent direct Lake Okeechobee discharge. Stations 5 and 6 captured outflow and inflow, respectively, of STA-2, FW 1. Station 2 was a sampling point approximately midway between Stations 5 and 6.

Samples were collected following Florida Department of Protection standard operating procedures in 20 L carboys which had been pre-rinsed with site water (FL-DEP, 2017). Carboys containing the samples were received on November 20, 2015 and stored in a walk-in cooler at 4 °C. Sample identification information on the carboys was recorded and samples were assigned lab numbers. Each sample was subsampled several times into smaller containers (1 L Nalgene bottles) to enable practical handling in the laboratory during subsequent processing. and immediately stored in a refrigerator at 4 °C. Samples were then filtered (0.45-μm nominal pore size) to separate particulate solids >0.45 μm for XRD analysis which took place between December 9–15, 2015. It was necessary to filter greater than 10 L to obtain sufficient particulate solids to enable analysis.

Mg saturation was performed for all samples to standardize interlayer expansion tendencies of expansible phyllosilicates, which can be highly influential on soil properties, for XRD analysis, should these minerals be present (Harris and White, 2008). Expansible phyllosilicates are clay minerals that can adsorb water and cations on their interior surfaces, conferring high cation exchange capacity relative to non-expansible minerals (Harris and White, 2008). Each sample was saturated with Mg by washing particulates with 1 M $MgCl_2$ while still on the filter, followed by rinsing with double deionized (DDI) water to remove any excess salt. The retained solids were transferred to a glass slide by placing the moist filter, retentate-side down, onto a glass slide and gently rolling a glass rod across the surface. The filter was then peeled away from the slide, leaving some of the retentate on the slide. The retentate that remained on the filter was gently scraped off using the edge of another glass slide. All recovered retentate was air-dried and transferred to a 7-mL glass scintillation vial and stored in a refrigerator for later analyses which were performed within a month.

The Mg-saturated samples were mounted for XRD analysis by placing them, in air-dried form, onto the surface of a quartz crystal mount. The quartz crystal is specially cut to minimize background relative to a glass slide. This was advantageous for these samples because of the small amount of particulate mass recovered. A drop of DDI water was added to each sample and the material was distributed about the surface of the quartz crystal in an area of approximately 1 cm^2 (about the area irradiated during XRD) using a small metal spatula. Samples were then allowed to dry prior to the XRD scan.

Another mounting approach was used to minimize the effects of coarse particles. Samples were immersed in a few mL of DDI water within a 7-mL scintillation vial, sonicated, and allowed to settle for ~15 s. About 2 mL of suspension was then withdrawn from the vial, being careful to avoid withdrawal of coarser particles that had settled. This suspension was deposited onto a quartz crystal mount and allowed to dry in preparation for XRD analyses. Materials mounted in this way, avoiding sand, are referred to as “fine”, whereas the other unfractionated samples are referred to as “whole”. The “fine” sample mounting technique fostered preferred orientation parallel to dominant crystal directions or planes, favoring the detection of minerals with platy, fibrous or lath-like crystal habits (Harris and White, 2008).

Glycerol solvation effects (diagnostic interlayer expansions of phyllosilicates; Harris and White, 2008) were evaluated by mist application to the mounted sample for all samples that had any discernible indication of expansible phyllosilicates. Diagnostic effects of limited heat treatment (110 °C) on interlayer collapse (Harris and White, 2008) were also evaluated where applicable.

2.2. STA recently accreted soils (RAS) sample collection, preparation, and characterization

Six soil samples were collected from STA-2 using a push core method (Osborne et al., 2013) in September 2016. Cores were 10 cm in diameter and, as RAS depth was variable, from 20 to 50 cm in depth. STA-2 is considered a well-performing STA, consistently achieving an outflow total P concentration of 20 μg L^{-1} or lower (Chimney, 2019; Reddy et al., 2020). Details of the STA-2 configuration and performance history can be found in Supporting Information. Three samples (inflow, midflow and outflow) were collected from each of two FWs within STA-2: FW 1 (predominantly EAV) and FW 3 (predominantly SAV). Prior to the construction of STA-2, FW 1 was not farmed, while FW 3 was previously farmed except 25% of the FW in the southeastern portion. The unfarmed portion of FW 3 is dominated by EAV, consisting

of cattail with patches of sawgrass. The top 10 cm of soil in FW 1 is highly organic.

Soil cores were extruded, sectioned and stored at 4 °C until the RAS section was air-dried in preparation for characterization. RAS is the material that has accumulated between the floc and pre-STA soil layer since the STAs became operational and is largely composed of particulate organic material and inorganic sediments (SFWMD, 2018). Samples were gently crushed to a powder in an agate mortar and pestle, and loosely packed as-is into cavity mounts for XRD analysis.

The total carbon content of the samples was measured with a Flash EA 1112 Elemental Analyzer (CE Instruments, Saddlebrook, NJ). Total P content was determined by heating samples at 550 °C and digesting in 6 N HCl acid and subsequent measurement of P in the digestates (USEPA, 1983). Total carbon and total P analyses included method duplicates, analytical spike recovery samples, as well as the analysis of an internal reference soil and an external reference material (National Institute of Standards and Technology 1547 Peach Leaves) with known P and carbon content.

2.3. XRD analysis

A computer-controlled X-ray diffractometer (Ultima IV X-Ray Diffractometer, Rigaku Corporation, Japan) equipped with stepping motor and graphite crystal monochromator was used to measure the mineral content of samples. Scans were conducted from 2 to 60° 2θ at a rate of 2 degrees 2θ per minute using Cu Kα radiation. Minerals were identified by referencing X-ray powder diffraction data for minerals published by the Joint Committee on Powder Diffraction Standards (JCPDS,(Mineral Powder Diffraction File Data Book, 1980).

2.4. SEM analysis of STA samples

SEM in conjunction with EDS was used to further probe the nature of P associations in the STA samples. These techniques provide direct solid-state determination of elemental associations within and between particles. STA sediment samples were applied as a dry powder onto C adhesive tape mounted on a cylindrical stub. The mounted powders were coated with a thin C film to promote electron conduction and minimize charge buildup on surfaces. The SEM imaging and EDS analyses (elemental spectra and dot maps) were conducted on either a FEI Nova NanoSEM 430 field emission SEM equipped with an EDS detector or a Tescan MIRA3 SEM, also with EDS detector.

2.5. Synchrotron-based μXRF analysis of STA samples

Air-dried RAS samples were shipped to Stanford Synchrotron Radiation Light Source (SSRL) in Palo Alto, CA. Samples were spread as an air-dried power onto P-free tape and mapped using a motor step size of 5 μm × 5 μm with a dwell time of 25 ms at Beamline 2–3. The two-crystal monochromator was calibrated at 7200 eV. Correlation plots illustrating the correlation between the presence of P and other elements including Ca, K, and Fe were generated using Sam's Microprobe Analysis Kit (SMAK) software version 1.5 (Webb, 2011).

2.6. XAS analysis of STA samples

RAS samples were also mounted, again on metal and P-free tape, and analyzed via X-ray absorbance spectroscopy (XAS) at Beamline 14–3 at the Stanford Synchrotron Radiation Lightsource (SSRL) in Palo Alto, CA. X-ray energy was scanned by a Silicon III phi 90 monochromator, calibrated to 2152.9 eV, with an energy resolution of 0.2 eV. Fluorescence was measured using a 4-element silicon drift diode detector. X-ray absorbance near-edge spectra (XANES) were collected for samples and a suite of organic and inorganic standards that included aluminum phosphate ($AlPO_4$), brushite ($CaHPO_4 * 2H_2O$), hydroxyapatite ($Ca_5(PO_4)_3(OH)$), monoammonium phosphate ($NH_4H_2PO_4$), phosphorus pentoxide (P_2O_5), organic P as Na-phytic acid, and iron phosphate dihydrate ($FePO_4{}^*2H_2O$). Spectra also were collected on goethite, gibbsite, kaolinite, and vermiculite treated with potassium phosphate dibasic (K_2HPO_4) using previously published methods (Schwertmann and Cornell, 1991). Standards were diluted with boron nitride, as needed, for analysis. Collected XANES spectra were processed using IFEFFIT software (Ravel and Newville, 2005).

3. Results and discussion

3.1. Mineralogical analyses

The most prevalent mineral components of suspended particulates in STA source water samples were either carbonates (calcite and dolomite) or quartz (SiO_2; Table 1). All samples contained calcite ($CaCO_3$). Dolomite [$CaMg(CO_3)_2$] was present, often abundantly, in all but one sample. Palygorskite [$(Mg, Al)_5(Si, Al)_8O_{20}(OH)_2 \cdot 8H_2O$] and sepiolite ($Mg_4(Si_6O_{15})(OH)_2 \cdot 6H_2O$) were identified in several samples, though the identification of sepiolite was less confident as a result of relatively low abundance. The presence of these minerals is consistent with previous work reporting calcite, sepiolite, palygorskite, dolomite, and quartz in sediment and suspended particulates in Lake Okeechobee and in water conveyances south of the lake (Harris et al., 2007). However, sepiolite was more prevalent and consistently present in the Lake Okeechobee particulate samples than in the samples being reported here. Pure minerals of the smectite group, which were also present in Lake Okeechobee particulates, were not confirmed in these outflow samples, but slight expansion and collapse of low-angle XRD peaks for Sample 4 (Fig. S2) suggest that smectite is present in minor amounts as a randomly-interstratified component with another phyllosilicate.

Preparation and analysis of the "fine" samples generally had the intended effect (Table 1). Most contained less quartz and exhibited less distortion of relative quartz XRD peak intensities relative to whole samples (Table 1). The peaks assigned to palygorskite, a mineral that typically features an elongated crystal habit, were more pronounced for the "fine" samples (Figs. S2–S3) than for the whole samples, possibly due to enhanced preferred orientation. Samples 2 and 5 were distinguished from other samples by lower suspended particulate concentrations, lighter color, and lack of any evidence for palygorskite.

Previously reported XRD analysis of STA RAS (Reddy et al., 2020) showed some continuity with the Okeechobee outflow suspended particulate mineralogy reported here, but there were also notable mineralogical distinctions between the two sources. Calcite was the dominant mineral component in all STA RAS samples (Table 2) and most Lake Okeechobee outflow samples (Table 1). Quartz also was found in some samples from both sources though it was generally less abundant

Table 1
Minerals filtered from source waters in either whole samples or in samples after allowing sand to settle. Minerals that were present in approximately equal amounts are indicated with ≈.

Source water sampling station	Dominant minerals present in whole sample (in descending abundance)	Dominant minerals present in sample after sand settling (in descending abundance)
1	Calcite, dolomite ≈ quartz, palygorskite, kaolinite, possible sepiolite	Calcite, palygorskite, dolomite ≈ quartz
2	Quartz, calcite, dolomite, kaolinite	Calcite, dolomite, kaolinite ≈ quartz
3	Dolomite, quartz, calcite, kaolinite, possible sepiolite	Calcite, palygorskite, dolomite ≈ quartz
4	Dolomite, calcite ≈ quartz, kaolinite, possible palygorskite and sepiolite	Dolomite, quartz, calcite ≈ kaolinite ≈ sepiolite, possible palygorskite
5	Quartz, calcite, kaolinite	Very small sample mass obtained; calcite and kaolinite detected
6	Calcite, dolomite ≈ quartz, possible palygorskite	Calcite, dolomite, palygorskite ≈ quartz, kaolinite

in the STA RAS. Aragonite ($CaCO_3$ polymorph of calcite) was detected in five of the six STA RAS samples but not in any sample of the Lake Okeechobee outflow particulates. Dolomite and palygorskite were present in most of the Lake Okeechobee samples but were much less prevalent among samples of STA RAS. Kaolinite and sepiolite were found in Lake Okeechobee outflow samples but not in any STA RAS samples.

Overall, the STA RAS samples were less mineralogically diverse than the particulates suspended in STA source waters. The former were more dominated by $CaCO_3$ (calcite and aragonite) but lacked or were nearly devoid of phyllosilicates (kaolinite, palygorskite, sepiolite) that were more abundant in the latter. Dominance of calcite and the reduction or disappearance of presumably Lake Okeechobee-derived components (dolomite and phyllosilicates) suggests a strong autochthonous influence on STA RAS accumulation, where photosynthetically driven $CaCO_3$ precipitation is likely a prevalent biogeochemical process. In a STA-1 W mesocosm study, this was seen with percent removal of Ca^{2+} following a similar trend as primary productivity. This positive correlation was most prevalent in an SAV system, where high pH had a significant influence on $CaCO_3$ precipitation and in all probability, the co-precipitation of calcium phosphates (Mitsch et al., 2015). All minerals identified in the STA source waters and STA RAS samples analyzed have been previously reported to occur in the Everglades (Das et al., 2012; Harris et al., 2007; Olila et al., 1995).

A trend was observed of increasing background and development of an "amorphous hump" (broad XRD peak typical of non-crystalline materials) in XRD data from the RAS from inflow to outflow in the EAV FW (Figs. S4–S6). These amorphous materials likely include OM and possibly biogenic silica (e.g., diatom frustules and sponge spicules) which increase from inflow to outflow regions of the FW (Table 2). OM and other non-crystalline components that may be present in the sample constitute diluents that significantly diminish the efficacy of XRD as a tool to detect and identify minerals. However, that effect was only a significant issue in the EAV FW outflow sample.

Phosphorus concentrations in STA RAS were small and no P minerals were detected via XRD in any of the samples from either FW. However, this does preclude the presence of P minerals at low concentrations. The EDS elemental spectra of the highest total P samples, inflow (1113 mg kg^{-1}; Fig. 2) and midflow (1114 mg kg^{-1}) from the EAV FW, showed Ca and P associations consistent with a discrete calcium phosphate mineral phase (Reddy et al., 2020). There could be more diffuse associations of P with Ca as well, as by sorption or substitution mechanisms, but this could not be confirmed by SEM/EDS. Elemental dot maps of the inflow (Fig. S7) and midflow samples of the SAV FW (Fig. S8) revealed no evidence of discrete Ca—P rich particles that were observed in the EAV FW. However, this may have been the result of the relatively low P concentrations (825 and 368 mg kg^{-1} for the inflow and midflow samples, respectively) in the samples or high concentrations of $CaCO_3$ in the SAV FW, which could mask relationships with P (Reddy et al., 2020).

3.2. XRF analysis of STA RAS

Correlation plots examining the relationship between P and other elements indicated a strong correlation between P and both Ca and K for the SAV FW (Fig. 3). The strength of this correlation did not change between inflow and outflow. No correlation between P and Fe was observed. Similar relationships were observed in the RAS from the EAV FW. However, the correlation between P and both Ca and K, while still relatively strong, deteriorated between inflow and outflow (Fig. 4). While the reason for the deterioration of these relationships is unclear, it may be the result of organic inputs with differing P:Ca and P:K ratios resulting from the biological activity within the wetland cells.

3.3. XAS analysis of STA RAS

All sample spectra lacked the pre-edge feature at 2148.9 eV, evident in the $FePO_4$ spectrum (Fig. 5), that suggests the presence of Fe (III)-P bonds (Kim et al., 2015). All sample spectra also featured the post-edge shoulder indicative of apatitic minerals, which was particularly well-resolved in the SAV FW inflow spectra. The absorption edge was also located at a slightly lower energy for all samples, similar to that observed in the reference spectrum for PO_4^{3-} adsorbed to alumina.

X-ray fluorescence mapping, which is more sensitive than SEM or XRD, confirmed that both Ca and K were strongly correlated with P in inflow and outflow sampling locations with both SAV (Fig. 3) and EAV (Fig. 4) FWs. That 3-dimensional Ca—P phase is likely a Ca phosphate mineral not present in sufficient concentration in these samples to be identified using XRD. The correlation between both K and Ca and P suggests that this P is present in its own 3-dimensional phase with a specific stoichiometry rather than being diffusely associated with $CaCO_3$, such as by sorption or co-precipitation. The lack of a similar relationship between Fe and P suggests that no discrete Fe—P phases are present.

XAS analysis of these samples suggests that this Ca—P mineral is apatitic in nature, while also indicating the possible presence of phosphate adsorbed to alumina and again providing no evidence that Fe—P phases are present. Both the lack of a relationship between Fe and P and the likely presence of apatite is consistent with earlier work, albeit work done on Lake Okeechobee sediments from a very different system than the STAs. This work demonstrated that Fe—P precipitation controls P behavior in aerobic surface water or soil conditions but that Ca—P precipitation is the controlling biogeochemical process in anaerobic conditions, such as those that RAS would experience (Moore and Reddy, 1994).

The source of the apatite detected in the STA RAS samples may be precipitation as a result of Ca and P present within groundwater and limestone parent material. The apatite might also be biogenic, with mechanisms for the biogenesis of apatite including bacterially-mediated synthesis (Kajander and Çiftçioglu, 1998), nucleation induced by anionic biomacromolecules (Dorvee and Veis, 2013) and bone deposition (Irick et al., 2013; Galbraith et al., 2010; Keenan and Engel, 2017). Bone deposition as a potential source is supported by the correlation of P with not only Ca, but also with K, as K can accumulate in bone, possibly being incorporated into bone crystal lattice in the X position in $Ca_9(PO_4)^*CaX_2$ (Bergstrom and Wallace, 1954; Wiesmann et al., 1998). However, for bone deposition to be the primary source of the apatitic minerals observed here, bones would have to have been deposited in a substantial and unlikely quantity.

Table 2
Locations and pertinent compositional data for stormwater treatment area 2 (STA-2) recently accreted soil (RAS) samples, as partially compiled from Reddy et al. (2020). Amorphous materials are likely dominated by organic matter but may also include biogenic silica.

Sample identification	Distance from inflow (m)	Total phosphorus (mean ± SE, mg kg^{-1})	Organic matter content (mean ± SE %)	Dominant minerals present (in descending abundance)
EAV Inflow (STA-2, FW 1)	400	1113 ± 264	66.3 ± 1.3	Calcite, aragonite, amorphous materials, possibly dolomite
EAV Midflow (STA-2, FW 1)	2700	1114 ± 389	79.9 ± 1.9	Calcite, amorphous materials, aragonite
EAV Outflow (STA-2, FW 1)	5200	814 ± 76	89.4 ± 0.2	Amorphous materials, calcite, quartz
SAV Inflow (STA-2, FW 3)	350	825 ± 123	23.1 ± 1.5	Calcite, aragonite, amorphous materials, possibly quartz and palygorskite
SAV Midflow (STA-2, FW 3)	2800	368 ± 72	26.3 ± 4.2	Calcite, aragonite, amorphous materials
SAV Outflow (STA-2, FW 3)	4450	375 ± 39	50.1 ± 2.4	Calcite, aragonite, amorphous materials, possibly quartz

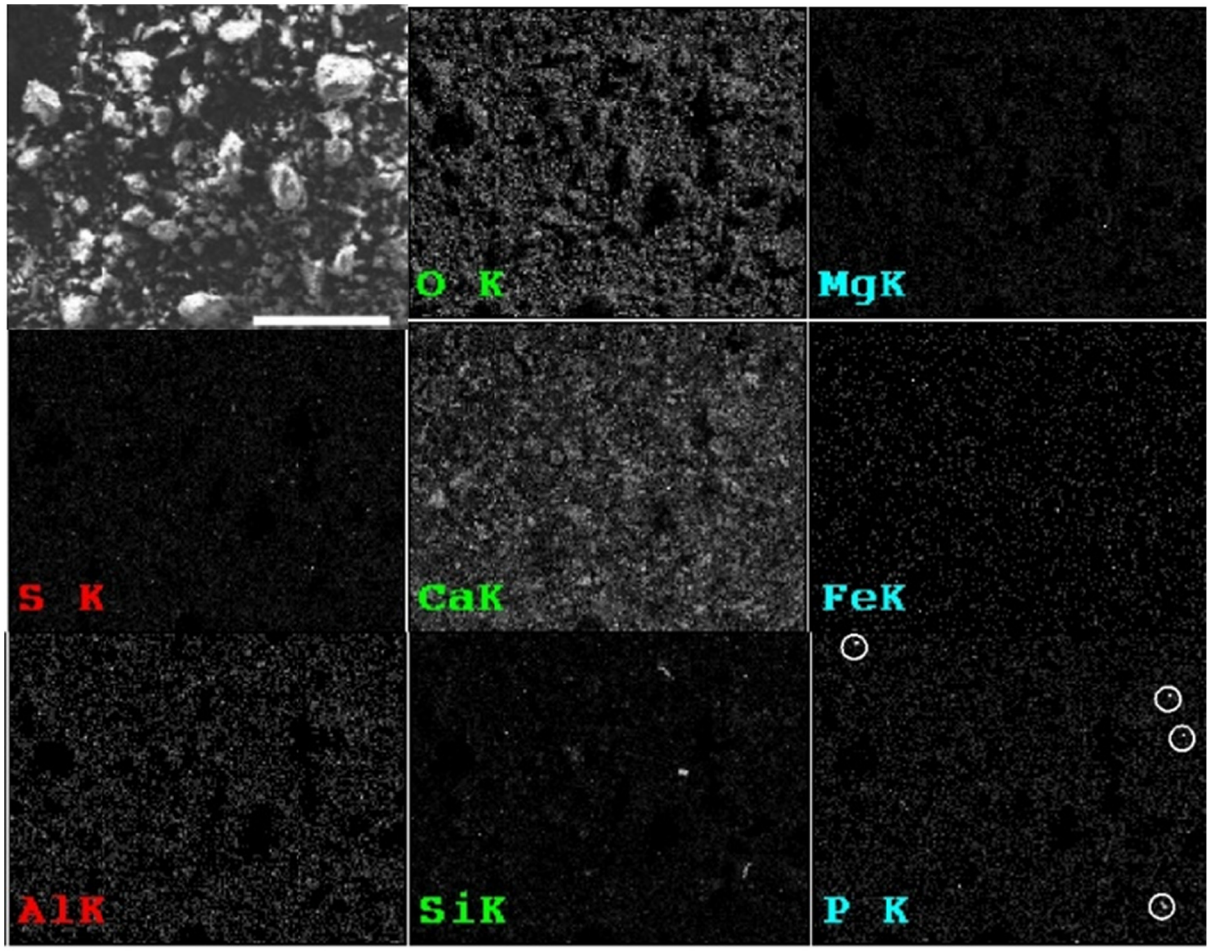

Fig. 2. Scanning electron microscopy (SEM) image (upper left; scale bar = 500 μm) and EDS-generated elemental dot maps (Kα radiation) for inflow sediments from emergent aquatic vegetation (EAV) FW. Bright pixels are indicative of relatively high concentration of a specific element. Wide distribution and abundance of Ca and O are evidenced by the relatively high/bright signal, consistent with dominance of $CaCO_3$ minerals as confirmed by XRD analysis. However, only small dots are indicated for P (lower right frame; highlighted by circles) at this magnification (100×). Similar SEM/EDS evidence for a Ca—P phase was reported on this sample by Reddy et al. (2020).

Relatively little work has been done attempting to characterize P in wetland soils using XAS. In the present study, the presumptive biogenic but crystalline nature of some of the mineral P phases present in these samples complicates attempts to quantitatively analyze the various P species present through approaches such as linear combination fitting. Defining organic P in these samples as the P similar to reference compounds such as Na-phytic acid and adenosine triphosphate, a common approach in soils, does not accurately capture, for example, biogenic apatite, and dramatically underestimates the organic P present in the sample compared to OM content measured by loss on ignition. In other work examining P speciation in wetland soils, findings similar to those presented here were described, with apatitic minerals being reported as present and no phases with Fe (III)-P being detected (Kim et al., 2015). These authors did not attempt linear combination fitting of these sample spectra. Linear combination fitting was also not attempted for peat soil samples by Kruse and Leinweber (2008), as the researchers viewed this approach to be unpromising considering the complex nature of the Al- and Fe-organic complexes they hypothesized to be present (Kruse and Leinweber, 2008).

Recently, work characterizing the P speciation of RAS within these same STA FWs via ^{31}P NMR and P fractionization techniques was reported (Reddy et al., 2020). P fractionization analysis indicated that highly reactive P, reactive P, and non-reactive P accounted for approximately 25–30, 50–60, and 15–20%, respectively, of the total P present. Within the HRP and RP pools, organic P was dominant in the EAV FW, whereas inorganic P was present in a larger concentration in the SAV FW. P concentrations in the EAV FW were higher compared to the SAV FW due to the accumulation of organic matter and associated nutrients, but the amount of P stored per unit area was significantly higher in the SAV FW. Reddy et al. (2020) also asserted that the organic P present was relatively refractory, consistent with potentially biogenic apatitic minerals. However, work examining biogenic phases in STA outflow water reported that biogenic P leaving the STAs was present in relatively labile phases such as orthophosphate diesters (DNA, RNA, and P lipids) and their degradation products (Jorgensen et al., 2015). The findings from these two studies combined with the present work suggest that relatively refractory particulate organic P phases may be effectively stored within the STAs.

In other recent studies, combinations of these advanced methods successfully determined soil chemical composition in relation to the storage of P in different soil types and ecosystems. For example, in the temperate forest landscape of Mt. Asma, Mie, Japan, P storage and cycling was found to be dependent on orthophosphate monoesters and P associated with Fe minerals using NMR, XAS and sequential chemical extractions (Hashimoto and Watanabe, 2014). In contrast to the STA RAS samples analyzed in the current work, XAS spectra showed an intense white line peak in a narrow energy range corresponding to spectral features exhibited when P is associated with Al and Fe minerals, with linear combination fitting indicating that phosphate adsorbed on ferrihydrite was the dominant P species in all samples. These data were supported by soil characterization which revealed that soils had elevated levels of Fe and Al.

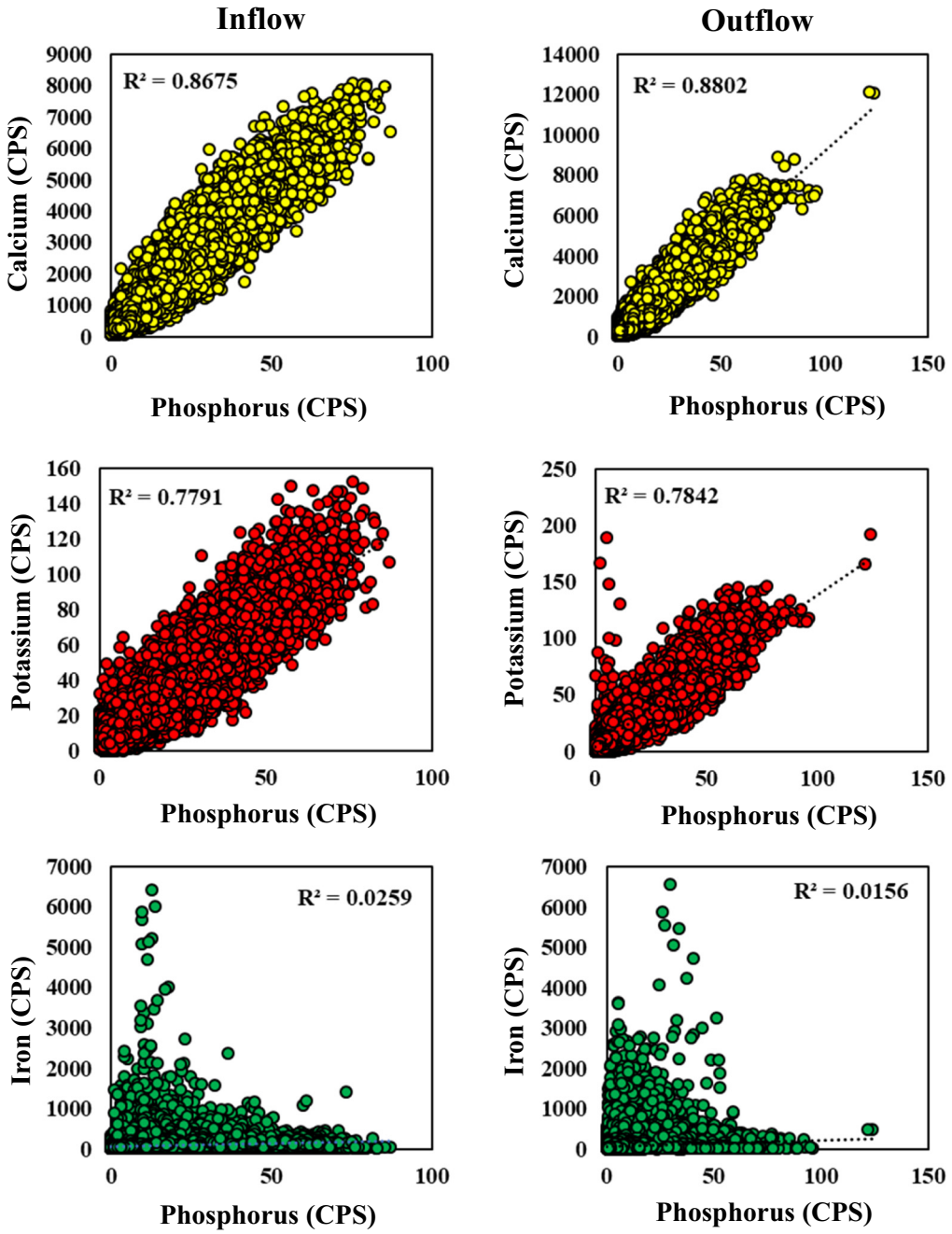

Fig. 3. Correlation plots, derived from X-ray fluorescence (XRF) data, for phosphorus, potassium, and iron within inflow (left) and outflow (right) recently accreted soil (RAS) of STA- 2, FW 3 (submerged aquatic vegetation; SAV) samples. Units for x and y axes are in counts per second (CPS).

Liu et al. (2017) were similarly successful at determining soil chemical composition, specifically in relation to legacy P storage and transformations, in high P soils historically fertilized with NK vs. NPK fertilizer and used for intensive agriculture. They determined that 27 years of maize cropping depleted soils of hydroxyapatite, while organic P was being accumulated through root and residue inputs and that $Ca(H_2PO_4)_2$ acted as the main reserve of labile P. ^{31}P NMR data showed this accumulation of organic P as inositol hexaphosphate dominated orthophosphate monoesters. Initial sequential extraction revealed that Ca_2—P increased 323% in soils amended with NPK, indicating that this pool may additionally be being depleted by maize uptake and subsequently being greatly enriched with P application. Results from XAS and μ-XRF indicated an accumulation of inositol hexaphosphate and Ca—P in NPK-fertilized soils compared to non-P fertilized soils and demonstrated an overlap of discrete Ca and P hotspots, whereas P was not correlated with Fe, Al or Si.

The work presented here indicates that the mineralogy of particulate material entering the STAs from Lake Okeechobee and the Everglades Agricultural Area basin consists largely of $CaCO_3$ minerals and quartz but that P minerals were undetectable within these particulates via XRD. The μXRF correlation plots presented here revealed that, within the STA FWs examined in the present study, P relationships with Ca and K in RAS near the FW inflow were very similar to P in RAS near the outflow in SAV FWs, whereas these relationships were altered more significantly between inflow and outflow in EAV FW. Furthermore, XANES and μXRF data suggest that the P present is associated with Ca and K and, in large part, apatitic in nature. These findings suggest the presence of biogenic apatite, although it remains uncertain what specific biogeochemical pathway(s) resulted in the accumulation of this specific apatitic material. Phosphorus was not associated with Fe in any of the samples analyzed here.

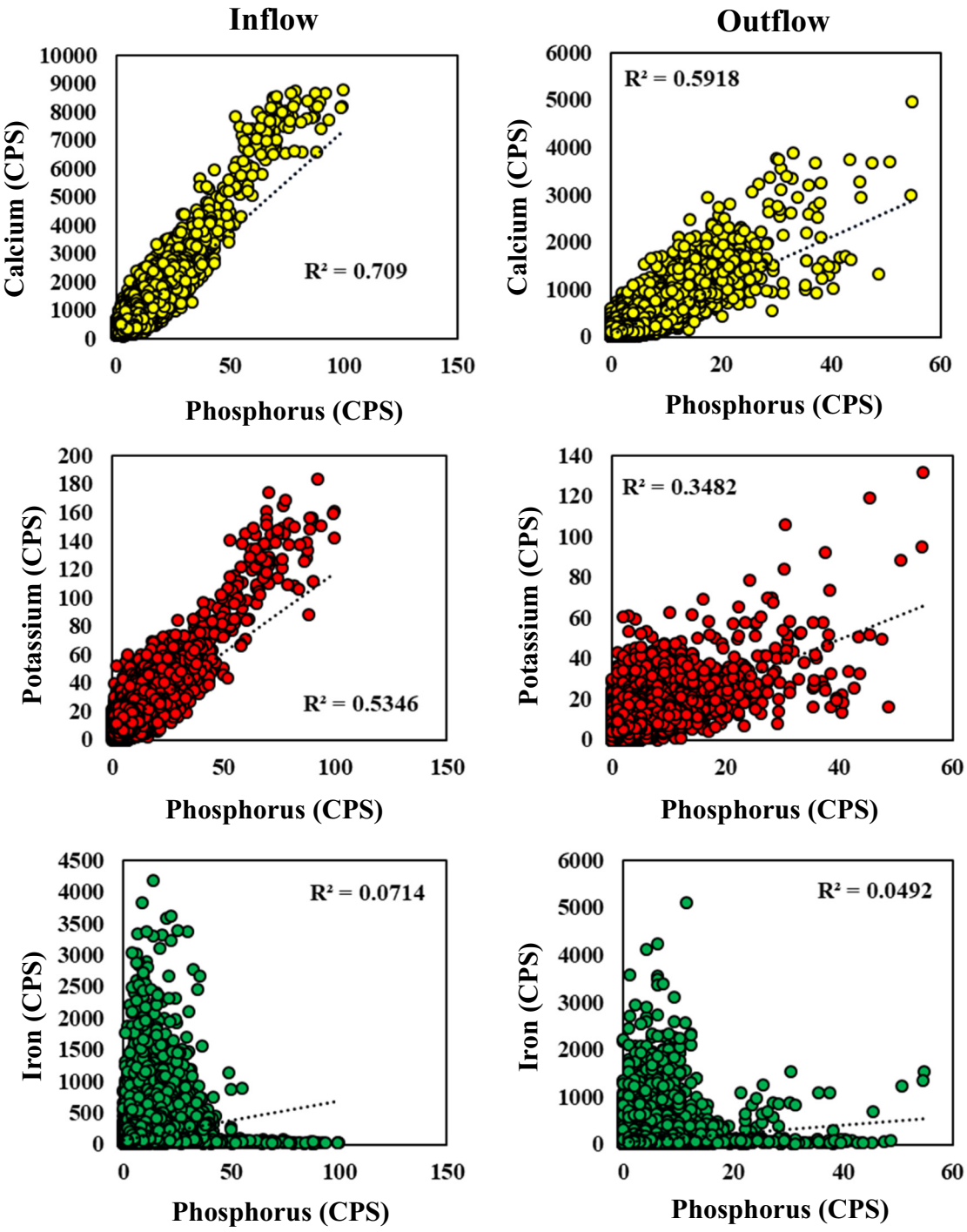

Fig. 4. Correlation plots, derived from X-ray fluorescence (XRF) mapping data, for phosphorus, potassium, and iron elements for inflow (left) and outflow (right) of STA-2, FW 1 (emergent aquatic vegetation; EAV) samples. Units for x and y axes are in counts per second (CPS).

Long-term P loading over the operational lifetime of STA-2 has increased the relative levels of all soil P types, with slowly available and refractory forms of organic P being the largest portion of P effectively stored. With only roughly a quarter of the total P in upstream areas of STA-2 being HRP, the key to the continuation of effective STA functioning is to maintain P-limiting conditions within the system to minimize P release into the water column for potential downstream transport (Reddy et al., 2020). Apatitic minerals, like those detected in the samples analyzed here, are likely to be relatively stable and only slowly available. As a result, these minerals would be less likely to perturb the sensitive oligotrophic ecosystems of the Everglades upon remobilization and transport downstream compared to more labile forms of P. Future work applying these techniques to samples from a greater number of STA FWs would be useful to examine these relationships more comprehensively, as would examination of the specific P—Ca and P—K relationships and XANES spectra for biogenic apatite generated from different biogeochemical pathways.

CRediT authorship contribution statement

Jonathan D. Judy: Writing – original draft, Investigation, Conceptualization, Methodology, Formal analysis, Funding acquisition. **Willie Harris:** Writing – original draft, Investigation, Conceptualization, Methodology,

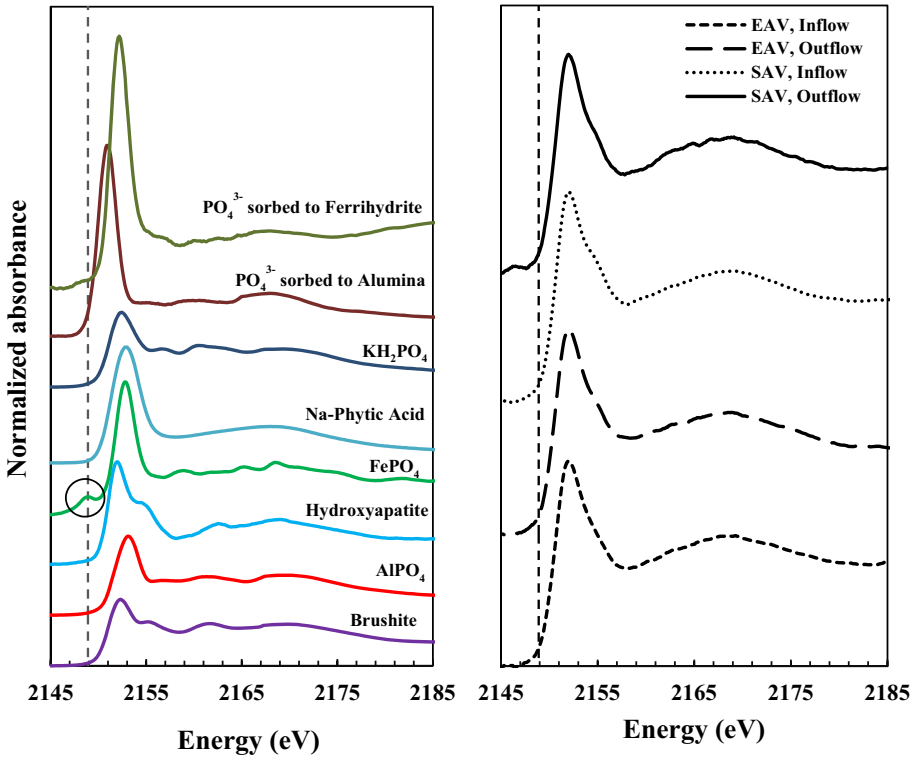

Fig. 5. X-ray absorption near-edge structure (XANES) spectra for reference materials (left) and samples (right). Pre-edge feature diagnostic of Fe—P bonds at 2148.9 eV, which is not evident in sample spectra, is indicated by dashed vertical line and circled. The post-edge shoulder that is evident in the hydroxyapatite reference (blue spectrum, left panel) is evident in the sample spectra, especially that of the SAV inflow sample.

Funding acquisition. **Ganga M. Hettiarachchi:** Methodology, Writing – review & editing. **A. Caroline Buchanan:** Writing – original draft, Writing – review & editing. **K. Ramesh Reddy:** Conceptualization, Methodology, Funding acquisition, Writing – review & editing.

Declaration of competing interest

The authors declare that they have no known competing financial interests or personal relationships that could have appeared to influence the work reported in this paper.

Acknowledgments

This research was supported in part by the funds provided by the South Florida Water Management District (SFWMD) under the contract UF-4600003031-WO01. It is part of the University of Florida Collaborative Research Initiative Science Plan with the SFWMD for the Everglades Stormwater Treatment Areas (CRESTA) and supports the Restoration Strategies Science Plan for the Everglades STAs. Dr. Judy was also partially supported by Hatch Project Accession Number 1014646 from the USDA National Institute of Food and Agriculture. We would like to thank Sam Webb, Erik Nelson, Sharon Bone and Nick Edwards for their assistance on the portion of this work conducted at beamlines 14-3 and 2-3 at the Stanford Linear Accelerator Laboratory. Authors appreciate the assistance of Odi Villapando (SFWMD) and Rupesh Bhomia (UF) for their assistance in collecting water and soil samples used in this study and Jill King, Cassondra Armstrong, Odi Villapando and Richard James from the SFWMD for providing feedback on the manuscript.

Appendix A. Supplementary data

STA configuration and performance details, XRD data, EDS spectra, SEM elemental dot maps. Supplementary data to this article can be found online at doi: https://doi.org/10.1016/j.scitotenv.2021.146740.

References

Bergstrom, W.H., Wallace, W.M., 1954. Bone as a sodium and potassium reservoir. J. Clin. Invest. 33, 867–873.
Bornette, G., Puijalon, S., 2011. Response of aquatic plants to abiotic factors: a review. Aquat. Sci. 73, 1–14.
Chen, H.J., Ivanoff, D., Pietro, K., 2015. Long-term phosphorus removal in the Everglades stormwater treatment areas of South Florida in the United States. Ecol. Eng. 79, 158–168.
Chimney, M.J., 2019. "South Florida Environmental Report, Chapter 5B: Performance and Operation of the Everglades Stormwater Treatment Areas." in. South Florida Water Management District, West Palm Beach, Florida.
Das, J., Daroub, S., Bhadha, J., Lang, T., Diaz, O., Harris, W., 2012. Physicochemical assessment and phosphorus storage of canal sediments within the Everglades Agricultural Area, Florida. J. Soils Sediments 12, 952–965.
Dorvee, J.R., Veis, A., 2013. Water in the formation of biogenic minerals: peeling away the hydration layers. J. Struct. Biol. 183, 278–303.
Farve, M., Harris, W., Dierberg, F., Portier, K., 2004. Association between phosphorus and suspended solids in an Everglades treatment wetland dominated by submersed aquatic vegetation. Wetl. Ecol. Manag. 12, 365–375.
FL-DEP, 2017. FS2100, Surface Water Sampling Tallahassee, Florida.
Galbraith, John M., Coultas, Charles L., Schwadron, Margo, O'Malley, Nina E., 2010. Bone phosphorus dominates fixed tree island soil in the Everglades WCA3. GEER 2010. Naples, FL.
Harris, W.G., White, G. Norman, 2008. X-ray diffraction techniques for soil mineral identification. In: Ulery, A.L., Drees, L.R. (Eds.), Methods of Soil Analysis: Mineralogical Methods. Part 5. Soil Science Society of America. Inc., Madison, WI.
Harris, W.G., Fisher, M.M., Cao, X., Osborne, T., Ellis, L., 2007. Magnesium-rich minerals in sediment and suspended particulates of South Florida water bodies: implications forTurbidity. J. Environ. Qual. 36, 1670–1677.
Hashimoto, Y., Watanabe, Y., 2014. Combined applications of chemical fractionation, solution P-31-NMR and P K-edge XANES to determine phosphorus speciation in soils formed on serpentine landscapes. Geoderma 230, 143–150.
Irick, D.L., Li, Y.C.C., Inglett, P.W., Harris, W.G., Gu, B.H., Ross, M.S., Wright, A.L., Migliaccio, K.W., 2013. Characteristics of soil phosphorus in tree island hardwood hammocks of the Southern Florida Everglades. Soil Sci. Soc. Am. J. 77, 1048–1056.
Jerauld, Michael, 2010. Factors Controlling Phosphorus Removal in Large Constructed Wetlands in South Florida. University of Florida, Gainesville, Fla.
Jorgensen, C., Inglett, K.S., Jensen, H.S., Reitzel, K., Reddy, K.R., 2015. Characterization of biogenic phosphorus in outflow water from constructed wetlands. Geoderma 257, 58–66.
Judy, J.D., Kirby, J.K., Farrell, M., McLaughlin, M.J., Wilkinson, S.N., Bartley, R., Bertsch, P.M., 2018. Colloidal nitrogen is an important and highly-mobile form of nitrogen discharging into the great barrier reef lagoon. Sci. Rep. 8, 12854.

Kadlec, R.H., 2006. Free surface wetlands for phosphorus removal: the position of the Everglades nutrient removal project. Ecol. Eng. 27, 361–379.
Kajander, E.O., Çiftçioglu, N., 1998. Nanobacteria: an alternative mechanism for pathogenic intra-and extracellular calcification and stone formation. Proc. Natl. Acad. Sci. 95, 8274–8279.
Keenan, S.W., Engel, A.S., 2017. Early diagenesis and recrystallization of bone. Geochim. Cosmochim. Acta 196, 209–223.
Kim, B., Gautier, M., Rivard, C., Sanglar, C., Michel, P., Gourdon, R., 2015. Effect of aging on phosphorus speciation in surface deposit of a vertical flow constructed wetland. Environ. Sci. Technol. 49, 4903–4910.
Kroger, R., Holland, M.M., Moore, M.T., Cooper, C.M., 2007. Plant senescence: a mechanism for nutrient release in temperate agricultural wetlands. Environ. Pollut. 146, 114–119.
Kruse, J., Leinweber, P., 2008. Phosphorus in sequentially extracted fen peat soils: a K-edge X-ray absorption near-edge structure (XANES) spectroscopy study. J. Plant Nutr. Soil Sci. 171, 613–620.
Lee, S.W., Kim, J.H., Cha, S.M., 2020. Analysis of the relation between pollutant loading and water depth flowrate changes in a constructed wetland for agricultural nonpoint source pollution management. Ecol. Eng. 152.
Li, D., Zheng, B.H., Liu, Y., Chu, Z.S., He, Y., Huang, M.S., 2018. Use of multiple water surface flow constructed wetlands for non-point source water pollution control. Appl. Microbiol. Biotechnol. 102, 5355–5368.
Liu, J., et al., 2017. Molecular speciation and transformation of soil legacy phosphorus with and without long-term phosphorus fertilization: Insights from bulk and microprobe spectroscopy. Scientific Reports 7.
Makris, K.C., Grove, J.H., Matocha, C.J., 2006. Colloid-mediated vertical phosphorus transport in a waste-amended soil. Geoderma 136, 174–183.
Mendes, L.R.D., Tonderski, K., Iversen, B.V., Kjaergaard, C., 2018. Phosphorus retention in surface-flow constructed wetlands targeting agricultural drainage water. Ecol. Eng. 120, 94–103.
Mineral Powder Diffraction File Data Book. 1980. JCPDS—International Center for Diffraction Data: PA, USA.
Mitsch, W.J., Zhang, L., Marois, D., Song, K., 2015. Protecting the Florida Everglades wetlands with wetlands: can stormwater phosphorus be reduced to oligotrophic conditions? Ecol. Eng. 80, 8–19.
Moore, P.A., Reddy, K.R., 1994. Role of eh and Ph on phosphorus geochemistry in sediments of Lake Okeechobee, Florida. J. Environ. Qual. 23, 955–964.
Moore, K.A., Shields, E.C., Parrish, D.B., Orth, R.J., 2012. Eelgrass survival in two contrasting systems: role of turbidity and summer water temperatures. Mar. Ecol. Prog. Ser. 448, 247–258.
Olila, O.G., Reddy, K.R., Harris, W.G., 1995. Forms and distribution of inorganic phosphorus in sediments of two shallow eutrophic lakes in Florida. Hydrobiologia 302, 147–161.
Osborne, T.Z., Ron, R.D., DeLaune, D., 2013. Soil and sediment sampling in inundated environments. In: DeLaune, R.D., Reddy, K.R., Richardson, C.J., Megonigal, P. (Eds.), Methods in Biogeochemistry of Wetlands. Soil Science Society of America Inc., Madison, Wisconsin, USA.
Pant, H.K., Reddy, K.R., 2001. Hydrologic influence on stability of organic phosphorus in wetland detritus. J. Environ. Qual. 30, 668–674.
Ravel, B., Newville, M., 2005. ATHENA, ARTEMIS, HEPHAESTUS: data analysis for X-ray absorption spectroscopy using IFEFFIT. J. Synchrotron Radiat. 12, 537–541.
Reddy, K.R., Vardanyan, L., Hu, J., Villapando, O., Bhomia, R.K., Smith, T., Harris, W.G., Newman, S., 2020. Soil phosphorus forms and storage in stormwater treatment areas of the Everglades: influence of vegetation and nutrient loading. Sci. Total Environ. 725, 138442.
Schwertmann, U., Cornell, R.M., 1991. Iron Oxides in the Laboratory: Preparation and Characterization. VCH Publ. Co., Weinheim, Germany.
SFWMD, 2018. Science Plan for the Everglades Stormwater Treatment Areas. South Florida Water Management District, West Palm Beach, Florida.
USEPA, 1983. Methods for Chemical Analysis of Water and Wastes: Method 365.1. Environ. Monit. Support Lab, Cincinnati, OH, USA.
Vymazal, J., 2007. Removal of nutrients in various types of constructed wetlands. Sci. Total Environ. 80, 48–65.
Webb, S.M., 2011. The MicroAnalysis Toolkit: X-Ray Fluorescence Image Processing Software. Amer. Inst. Phys. Conf. Proc.
Wiesmann, H.P., Plate, U., Zierold, K., Höhling, H.J., 1998. Potassium is involved in apatite biomineralization. J. Dent. Res. 77, 1654–1657.
Wilber, D.H., Clarke, D.G., 2001. Biological effects of suspended sediments: a review of suspended sediment impacts on fish and shellfish with relation to dredging activities in estuaries. N. Am. J. Fish Manag. 21, 855–875.
Xing, Y., Chen, X., Chen, X., Zhuang, J., 2016. Colloid-mediated transport of pharmaceuticals and personal care products through porous media. Sci. Rep. 6, 35407.